# Phase Diagram of Fluid Vesicles

G. Gompper[1] and D. M. Kroll[2]

[1]*Sektion Physik der Ludwig-Maximilians-Universität München, Theresienstrasse 37, 80333 München, Germany*
[2]*Department of Medicinal Chemistry and Minnesota Supercomputer Institute, University of Minnesota, 308 Harvard Street SE, Minneapolis, Minnesota 55455*

The phase diagram of self-avoiding fluid vesicles as a function of the bending rigidity $\kappa$ and the pressure increment $p$ is studied using Monte Carlo simulations and scaling arguments. For $p > 0$, a line of first-order transitions is observed between a branched-polymer-like phase and an inflated phase. The first-order line ends at small positive $p$; it extends to negative $p$ as a line of compressibility maxima. For $p < 0$, and sufficiently large $\kappa$, stomatocytes are stable. The scaling behavior as a function of system size is markedly different for positive and negative $p$.

PACS numbers: 87.22.Bt, 05.40.+j, 64.60.Fr

The thermal behavior of membranes and vesicles has recently attracted a great deal of attention [1–3]. Membranes are (approximately) incompressible two-dimensional films composed of amphiphiles or lipids which—on experimentally relevant time scales—do not change their area. For this reason, the shape and fluctuations of membranes are controlled by their bending rigidity [4] rather than by a surface tension as is the case for interfaces. Theoretical and experimental work on vesicles has been restricted almost exclusively to membranes with a very large bending rigidity $\kappa$, where thermal fluctuations are of only minor importance [5]. Very little is known about the behavior of vesicles in the low-bending-rigidity regime [6].

The two intensive thermodynamic fields which determine the conformation and structure of vesicles are the bending rigidity $\kappa$ and the pressure difference $p = p_{in} - p_{out}$ between the vesicle interior and exterior. $p$ is the thermodynamic variable conjugate to the enclosed volume $V$. The behavior of self-avoiding low-bending-rigidity vesicles has been studied theoretically as a function of $\kappa$ for $p = 0$ [7,8], and as a function of $p$ for $\kappa = 0$ [9]. In the first case, a peak in the specific heat is observed at $\kappa \simeq k_B T$, the interpretation of which is the subject of intense current debate [7,10–12]. The question which arises is whether there is a phase transition separating a low-bending-rigidity, branched-polymer-like phase [7,8,13,14] from a high-bending-rigidity, extended phase. For $\kappa = 0$, a first-order transition is observed between a low-pressure, branched-polymer-like phase and a high-pressure, inflated phase [9]. Experimentally, low-bending-rigidity vesicles have been shown to be able to penetrate through the intact skin [15], and may thus have a large number of applications in medicine, biotechnology, and other areas.

In this paper, we present the results of extensive Monte Carlo simulations for the phase diagram of fluid vesicles as a function of the bending rigidity $\kappa$ and (positive and negative) pressure increment $p$. The model we study consists of $N$ hard spheres of diameter $\sigma = 1$, which are connected by flexible tethers of length $l_0 = \sqrt{2.8}$ to form a two-dimensional network of spherical topology. This choice of $l_0$ ensures self-avoidance. In order to allow for diffusion within the membrane, and thus to describe fluid membranes, tethers can be cut and reattached between the four beads which form two neighboring triangles [16,17]. A Monte Carlo step (MCS) then consists of an attempt to update the positions of all $N$ beads by a random increment in the cube $[-s, s]^3$, followed by $N$ attempted tether cuts. We chose $s = 0.15$ so that approximately 50% of the attempted coordinate updates were successful. The bending elastic energy is [18,19]

$$\mathcal{H}/k_B T = \kappa \sum_{\langle ij \rangle} (1 - \mathbf{n}_i \cdot \mathbf{n}_j), \tag{1}$$

where $\mathbf{n}_i$ is the unit normal vector of triangle $i$, and the sum runs over all pairs of neighboring triangles. Averages are typically calculated over runs of $20 \times 10^6$ MCS. Details of our simulation procedure can be found in Ref. [7].

The $\kappa$-$p$ phase diagrams for systems consisting of $N = 127$ and $N = 247$ beads are shown in Fig. 1. The first-order transition observed previously [9] at $\kappa = 0$ persists to finite values of $\kappa$. With increasing $\kappa$, the transition occurs at lower and lower values of $p$, since both the bending rigidity and the (positive) pressure act to increase the volume of the vesicle. This first-order transition is characterized by a bimodal probability distribution function $P(V)$ for the volume. We locate the transition at the point where the two maxima in $P(V)$ are of equal height. These maxima approach each other with increasing $\kappa$, and merge into a single peak at $\kappa \simeq 0.32$ for $N = 127$, $\kappa \simeq 0.45$ for $N = 247$, and $\kappa \simeq 0.52$ for $N = 407$. Thus, the line of first-order transitions extends to higher values of $\kappa$ for larger systems sizes. For values of $\kappa$ beyond this "critical" point, we find a line of maxima of the compressibility $\chi = \langle V \rangle^{-1} \partial \langle V \rangle / \partial p$. This line extends to the highest value of $\kappa$ studied in this paper, $\kappa = 6$. It crosses the $\kappa$ axis at $\kappa \simeq 1.0$ for $N =$
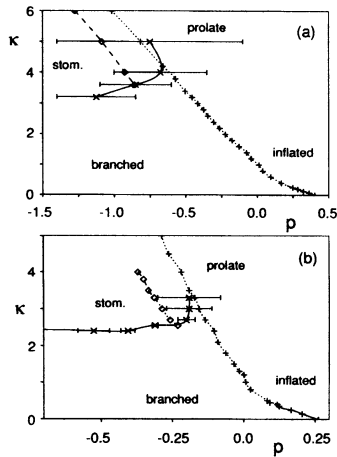
FIG. 1. Phase diagram of fluid vesicles as a function of pressure increment $p$ and bending rigidity $\kappa$, for (a) $N = 127$ and (b) $N = 247$. First-order transitions are denoted by solid lines, compressibility maxima by dotted lines. The dumbbell-metastable disocyte transitions are shown as a dashed line. The error bars span the spinodals for the transition to stomatocytes. The solid line through their midpoints serves as a guide to the eye.

127 and $\kappa \simeq 1.2$ for $N = 247$. For larger $\kappa$, there is a rapid change in the vesicle shape, from roughly spherical prolate to dumbbell, as this line of susceptibility maxima is crossed with decreasing $p$. A few typical configurations are shown in Fig. 2.

For large $\kappa$ and sufficiently *negative* pressures, stomatocytes are found to be stable. Stomatocytes decay with increasing pressure into dumbbels, and with decreasing $\kappa$ into branched-polymer-like shapes. The transition at large $\kappa$ is very strongly first order, and therefore cannot be localized easily. The error bars shown in Fig. 1 span the spinodal lines. Stomatocytes are also unstable at large negative pressures with respect to flat, pancake-shaped configurations since the latter have a smaller volume in our model. In the limit of very large negative pressures these pancakes transform smoothly into branched-polymer-like configurations. The lowest value of $\kappa$ for which stomacotyes are stable is $\kappa \simeq 3.1$ for $N = 127$ and $\kappa \simeq 2.4$ for $N = 247$. The region of stability of stomatocytes therefore extends to *smaller* values of $\kappa$ for larger system sizes.

We also see discocytes, but it appears that they are only metastable, and always decay into stomatocytes. Nevertheless, we do observe a transition between discocytes and prolate, dumbbell-shaped vesicles. There is a line of first-order transitions between these two phases for large $\kappa$, which ends in a *lower* critical point located at $\kappa \simeq 3.5$ for $N = 127$ and $\kappa \simeq 3.3$ for $N = 247$; the critical point therefore moves to lower $\kappa$ with increasing system size. A line of compressibility maxima extends beyond this critical point; however, it is very short and never approaches the line of compressibility maxima mentioned above.

An analysis of vesicle shapes in the low-temperature limit [20] implies that the correct scaling variable in the large-$\kappa$ regime is the reduced pressure $\tilde{p} = pV_{\text{sphere}}/\kappa \sim$
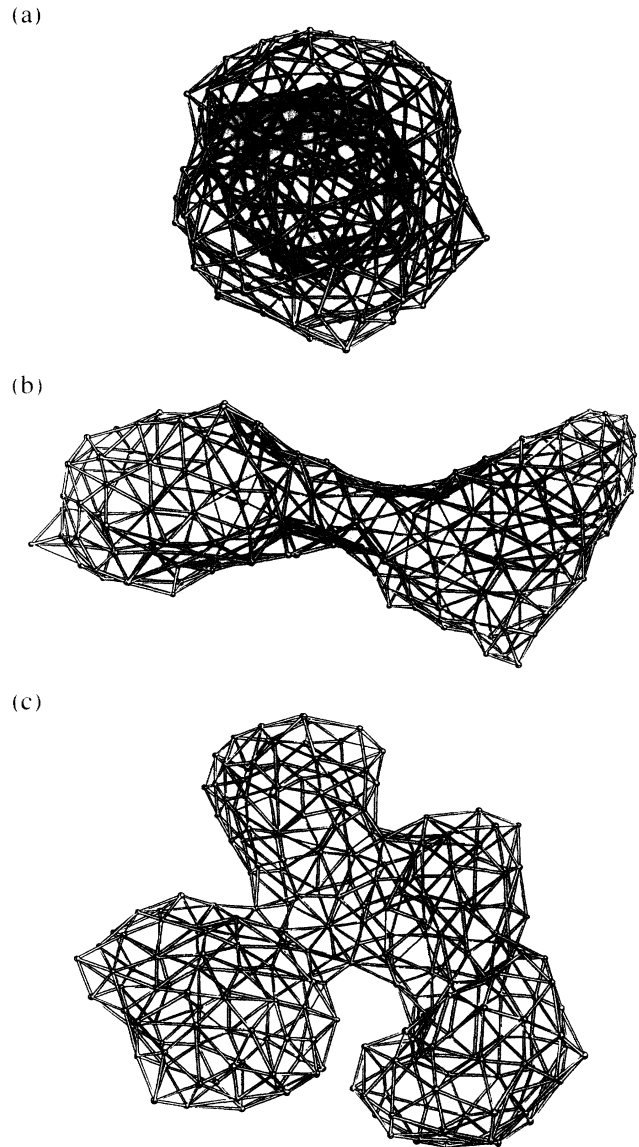


FIG. 2. Typical configurations of vesicles with $N = 247$ monomers. (a) $\kappa = 3.0$, $p = -0.27$ (stomatocyte); (b) $\kappa = 2.4$, $p = -0.19$ (dumbbell); and (c) $\kappa = 2.4$, $p = -0.35$ (branched polymer).

$pN^{3/2}\kappa^{-1}$. Phase transitions should occur at $\tilde{p} = \text{const}$. The scaling behavior of both the discocyte-dumbbell transitions and the line of compressibility maxima for $p < 0$ are consistent with this prediction. The peak height, $\chi_{\text{max}}$, of the compressibility along this line scales as $\chi_{\text{max}} \sim N^{-\gamma}$, with $\gamma = 1.35 \pm 0.05$ for $p < 0$. Although this seems to imply that a continuous phase transition occurs in the thermodynamic limit on crossing this line, more work is needed to verify this possibility.

The large-$\kappa$ portion of our phase diagram differs from that obtained by minimizing the bending energy in the pressure ensemble [21], where only a single transition from spheres to prolates is found with decreasing $p <$

0. In this ensemble, stable non-self-intersecting $T = 0$ configurations cease to exist before other shape transitions can occur. We find much better agreement with the $T = 0$ analysis of vesicle shapes in the volume ensemble [20], where a transition from stomatocytes to discocytes occurs at a reduced volume $v \equiv V/V_{\text{sphere}} = 0.59$, and a transition from discocytes to dumbbells at $v = 0.65$. This can be seen in Fig. 3, where we plot the phase diagram as a function of $\kappa$ and the reduced volume $\tilde{v} = \beta \langle V \rangle (N - 2)^{-3/2}$. Here, $\beta = 3^{1/4} 2^{5/2} \pi^{1/2} \langle l \rangle^{-3}$ is a constant, and $\langle l \rangle = 1.35$ is the average distance between neighboring beads [22]. The good agreement between our results and the phase diagram obtained by minimizing the bending energy in the volume ensemble is due to the fact that the effects of both self-avoidance and thermal fluctuations are included in our analysis.

The scaling behavior in the small-$\kappa$ portion of the phase diagram is different. We have argued in Ref. [9] that for $\kappa = 0$ the crumpled-to-inflated transition occurs at $\bar{p} = pN^\mu = \text{const}$, with $\mu = 1/2$. This is consistent with the data presented in Ref. [9] when a "shift variable" $N_0$ is introduced to account for the leading corrections to scaling [23], so that $\bar{p} = p(N - N_0)^\mu$. We find here that this scaling behavior holds not only for $\kappa = 0$, but along the whole line of first-order crumpled-to-inflated transitions. Furthermore, data taken along the line of compressibility maxima for $\kappa < 1.0$ also scale in this way. When no shift variable is used, our data scale best with $\mu = 0.65 \pm 0.05$. With the present range of vesicles sizes, however, it is not possible to distinguish between these two estimates for $\mu$.

In the inflated phases, for $\kappa = 0$, the volume was found in Ref. [9] to scale as

$$\langle V \rangle = p^{3\omega} N^{3\nu_+}, \quad \text{with} \quad \omega = \frac{1 - \nu}{3\nu - 1}, \quad \nu_+ = \frac{\nu}{3\nu - 1}, \tag{2}$$

with an exponent $\nu \simeq 0.79$, so that $3\omega = 0.47 \pm 0.01$ and $3\nu_+ = 1.735 \pm 0.005$. We have therefore calculated $\langle V \rangle$ as a function of $p$ in the inflated phase, for $\kappa = 0.50$ and $\kappa = 1.0$, with vesicle sizes $N = 247$ and $N =$
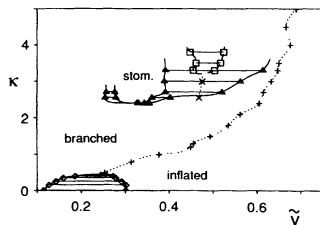


FIG. 3. Phase diagram of fluid vesicles in the pressure ensemble, as a function of reduced average volume $\tilde{v} = \beta \langle V \rangle (N - 2)^{-3/2}$, with $\beta = 3^{1/4} 2^{5/2} \pi^{1/2} \langle l \rangle^{-3}$, and bending rigidity $\kappa$, for $N = 247$. Compressibility maxima are denoted by dotted lines, the dumbbell-metastable disocyte transitions by a dashed line. The solid line in Fig. 1(b) has been used to estimate the average volume $\langle V \rangle$ at the transition to stomatocytes.

407. For $\kappa = 0.50$, we find that $3\omega = 0.42 \pm 0.02$ and $3\nu_+ = 1.718 \pm 0.010$, in agreement with Eq. (2). Taking into account that the range of pressures for which the data scale decreases with increasing $\kappa$, we believe that this value for $\omega$ is consistent with that obtained for $\kappa = 0$. Our results therefore support the conclusion that the scaling behavior in the inflated phase near the line of crumpled-to-inflated transitions is described by a single, universal exponent $\nu \simeq 0.79$. For $\kappa = 1.0$, we find $3\omega = 0.265 \pm 0.02$ and $3\nu_+ = 1.653 \pm 0.010$, which is considerably smaller than the values obtained at smaller $\kappa$ [but still consistent with the scaling relation $2\nu_+ = 1 + \omega$ implied by Eq. (2)]. However, data taken for this value of $\kappa$ probably lie outside the small-$\kappa$ scaling regime.

Finally, a rough estimate for location of the line of transitions from stomatocytes to crumpled configurations can be obtained as follows. Assume that the branched-polymer-like configurations are made of thin cylindrical arms of radius $\xi$. The free energy can then be approximated as

$$\mathcal{F}_{\text{bp}}/k_B T = -M \ln(z) + \frac{3}{2} \ln(M) - p \langle V \rangle$$
$$+ \frac{1}{2} \kappa \left\langle \int_A dA (c_1 + c_2)^2 \right\rangle$$
$$+ \bar{\kappa} \left\langle \int_A dA \, c_1 c_2 \right\rangle, \tag{3}$$

where $A \sim N$ is the surface area, $c_1$ and $c_2$ are the local principle curvatures, $z$ is a $N$-independent constant, and $M = A/2\pi\xi^2$ is the equivalent number of "monomers" of a branched polymer. The first two terms in Eq. (3) are the branched polymer entropy, while the last two terms give the average bending energy and the average Gaussian curvature. The average volume is $\langle V \rangle \simeq A\xi/2$. The bending energy is estimated to be $\kappa_R(\xi)A\xi^{-2}/2$, where $\kappa_R(\xi) = \kappa - (3/4\pi)\ln(\xi/a)$ is the renormalized bending rigidity [24] at length scale $\xi$. Here, $a$ is of the order of the tether length $l_0$. Finally, the average Gaussian curvature term is given approximately by $4\pi\bar{\kappa}_R(\xi)$, where $\bar{\kappa}_R(\xi) = \bar{\kappa} + (5/6\pi)\ln(\xi/a)$ is the renormalized saddle-splay modulus [25]. Since the surface area is held constant, the only variable in $\mathcal{F}_{\text{bp}}$ is the arm radius $\xi$, which is determined by minimizing the free energy.

The free energy of a stomatocyte of radius $R$, on the other hand, can be estimated as

$$\mathcal{F}_{\text{stom}}/k_B T = 2[8\pi\kappa_R(R)] + 4\pi\bar{\kappa}_R(R) + f_{\text{neck}} - p \langle V \rangle$$
$$+ c_\infty \frac{A}{\kappa} d^{-2}, \tag{4}$$

where the first term is the average bending energy of the inner and the outer shell of the stomatocyte, with $R^2 = A/8\pi$, the second term is the average Gaussian curvature contribution, the third (constant) term the bending energy of the neck region, and the last term the steric repulsion

[26] between the two shells at distance $d$, with an amplitude $c_x$. This approximation should be valid for $d$ much smaller than the vesicle radius $R$. The average volume is estimated to be $\langle V \rangle = Ad/2$. The only variable in this case is the distance $d$, which is again calculated by minimizing the free energy.

The results for the location of transitions from stomatocytes to crumpled configurations obtained using this approximation reproduce the main features seen in Fig. 1. The transition line shifts to lower values $\kappa$ with increasing $N$; simultaneously its pressure dependence becomes weaker. The analysis also indicates that a limiting form of the transition line is reached rather quickly with increasing system size, so that our Monte Carlo results for $N = 247$ can be expected to be close to the thermodynamic limit.

It would be very useful if these results could be compared with experiments on low-bending-rigidity vesicles. It seems that the best possibility for obtaining large vesicles with bending rigidities of order $k_B T$, which are stable on experimental time scales, is to use mixtures of either a lipid with a short-chain amphiphile [27] or of two lipids with different spontaneous curvatures [28]. Mixtures have the additional advantage that the value of $\kappa$ can be tuned by changing the composition of the membrane [28,29]. Indeed, the only current experiments with low-bending-rigidity vesicles have utilized these methods [15,30].

[1] *Statistical Mechanics of Membranes and Surfaces*, edited by D. R. Nelson, T. Piran, and S. Weinberg (World Scientific, Singapore, 1989).

[2] R. Lipowsky, Nature (London) **349**, 475 (1991).

[3] M. Bloom, E. Evans, and O. G. Mouritsen, Q. Rev. Biophys. **24**, 293 (1991).

[4] P. B. Canham, J. Theor. Biol. **26**, 61 (1970); W. Helfrich, Z. Naturforsch. **28c**, 693 (1973); E. Evans, Biophys. J. **14**, 923 (1974).

[5] M. Wortis, U. Seifert, K. Berndl, B. Fourcade, L. Miao, M. Rao, and R. K. P. Zia, in *Dynamical Phenomena at Interfaces, Surfaces and Membranes*, edited by D. Beysens, N. Boccara, and G. Forgacs (Nova Science, Commack, NY, 1991).

[6] The behavior of vesicles in *two* dimensions (ring polymers) has been addressed by C. J. Camacho, M. E. Fisher, and R. R. P. Singh, J. Chem. Phys. **94**, 5693 (1991), and references therein.

[7] D. M. Kroll and G. Gompper, Science **255**, 968 (1992).

[8] D. Boal and M. Rao, Phys. Rev. A **45**, R6947 (1992).

[9] G. Gompper and D. M. Kroll, Europhys. Lett. **19**, 581 (1992); Phys. Rev. A **46**, 7466 (1992).

[10] M. Bowick, P. Coddington, L. Han, G. Harris, and E. Marinari, Nucl. Phys. **B394**, (1993); K. Anagnostopoulos, M. Bowick, P. Coddington, M. Falconi, L. Han, G. Harris, and E. Marinari, Phys. Lett. B **317**, 102 (1993).

[11] J. Ambjørn, A. Irbäck, J. Jurkiewicz, and B. Petersson, Nucl. Phys. **B393**, 571 (1993).

[12] The simulations of Refs. [10,11] are for surfaces *without* self-avoidance.

[13] D. M. Kroll and G. Gompper, Phys. Rev. A **46**, 3119 (1992)

[14] C. F. Baillie and D. A. Johnston, Phys. Lett. B **293**, 55 (1992).

[15] G. Cevc and G. Blume, Biochim. Biophys. Acta **1104**, 226 (1992).

[16] A. Billoire and F. David, Nucl. Phys. **B275**, 617 (1986); D. V. Boulatov, V. A. Kazakov, I. K. Kostov, and A. A. Migdal, Nucl. Phys. **B275**, 641 (1986).

[17] J.-S. Ho and A. Baumgärtner, Europhys. Lett. **12**, 295 (1990); A. Baumgärtner and J.-S. Ho, Phys. Rev. A **41**, 5747 (1990).

[18] Y. Kantor and D. R. Nelson, Phys. Rev. Lett. **58**, 2774 (1987).

[19] The bending rigidity in the continuum limit, $\bar{\kappa}$, is related to $\kappa$ in Eq. (1) by $\bar{\kappa} = \kappa/\sqrt{3}$, see Ref. [7].

[20] K. Berndl, J. Käs, R. Lipowsky, E. Sackmann, and U. Seifert, Europhys. Lett. **13**, 659 (1990); U. Seifert, K. Berndl, and R. Lipowsky, Phys. Rev. A **44**, 1182 (1991).

[21] U. Seifert and R. Lipowsky, Phys. Rev. A **42**, 4768 (1990).

[22] $\langle l \rangle$ differs by only a few percent in various portions of the phase diagram.

[23] C. J. Camacho and M. E. Fisher, Phys. Rev. Lett. **65**, 9 (1990).

[24] L. Peliti and S. Leibler, Phys. Rev. Lett. **54**, 1690 (1985).

[25] H. Kleinert, Phys. Lett. **114A**, 263 (1986).

[26] W. Helfrich, Z. Naturforsch. **33a**, 305 (1978).

[27] M. M. Kozlov and W. Helfrich, Langmuir **8**, 2792 (1992).

[28] S. Leibler and D. Andelman, J. Phys. (Paris) **48**, 2013 (1987); S. A. Safran, P. Pincus, and D. Andelman, Science **248**, 354 (1990).

[29] U. Seifert, Phys. Rev. Lett. **70**, 1335 (1993); F. Jülicher and R. Lipowsky, Phys. Rev. Lett. **70**, 2964 (1993).

[30] H. P. Duwe, J. Käs, and E. Sackmann, J. Phys. (Paris) **51**, 945 (1990).

FIG. 2. Typical configurations of vesicles with $N = 247$ monomers. (a) $\kappa = 3.0$, $p = -0.27$ (stomatocyte); (b) $\kappa = 2.4$, $p = -0.19$ (dumbbell); and (c) $\kappa = 2.4$, $p = -0.35$ (branched polymer).